Petroleum Science 23 (2026) 5693–5705

Contents lists available at ScienceDirect

Petroleum Science

journal homepage: www.keaipublishing.com/en/journals/petroleum-science

Original Paper

Cooperative optimization of well-spacing and fracturing in tight reservoirs

Wen-Sheng Wu [a], Bo-Wei Zhang [b], Shi-Kai Tong [c], Xiu-Kun Wang [a,*]

[a] State Key Laboratory of Petroleum Resources and Engineering, China University of Petroleum (Beijing), Beijing, 102249, China
[b] National Key Laboratory of Underwater Acoustic Technology, Harbin Engineering University, Harbin, 150001, Heilongjiang, China
[c] Associated Gas Comprehensive Utilization Project Department of Changqing Oilfield Company, Xi'an, 710018, Shaanxi, China

ARTICLE INFO

Article history:
Received 20 December 2025
Received in revised form
7 February 2026
Accepted 13 April 2026
Available online 17 April 2026

Edited by Meng-Jiao Zhou

Keywords:
Tight oil
Integrated workflow
Well spacing
Fracturing intensity
Machine learning

ABSTRACT

The recovery factor of tight oil reservoirs is comprehensively controlled by formation geological properties, well spacing, and fracturing intensity. Insufficient formation drainage or fracture-hits between wells can lead to low recovery factors. The integrated optimization of well spacing and fracturing intensity is a crucial approach to improving recovery factors in tight oil reservoirs. This work analyzes the production characteristics of tight oil wells and identifies the main factors affecting productivity applying machine learning methods. An integrated workflow combining fracturing modeling, reservoir simulation, and production optimization is developed and applied to a real field reservoir block to explore the optimal matching relationship between well spacing and fracturing intensity. The research results indicate that the fractured horizontal well productivity is highly correlated with the stable water cut and is influenced by reservoir geological parameters and fracturing intensity. The material balance method can quickly reconstruct water saturation field after fracturing, which improves history matching. Moreover, simple machine learning method, response surface experiments, is used along with our integrated workflow to generate well spacing and fracturing intensity matching charts under different reservoir permeability conditions and provided the corresponding recovery factor prediction correlations. This study offers a fast and efficient method for developing tight oil reservoir with optimized well spacing and fracturing intensity.

1. Introduction

Tight oil reservoirs, as a tremendous unconventional resource to supplement conventional oil reservoirs and ensure future oil supply, are of great significance for their rational and efficient development (Conti et al., 2016). Compared to conventional reservoirs, tight oil reservoirs have inferior reservoir properties, low permeability, and high flow resistance, requiring the use of horizontal wells combined with hydraulic fracturing technique for development (Zhang et al., 2016; Liu, 2023). Multiple field cases have shown that while production rates from tight oil wells are initially high after hydraulic fracturing, they decline rapidly, and the elastic recovery factor is low (Male and Duncan, 2022; Luo and Su, 2022). In fact, the development effectiveness of tight oil reservoirs is influenced by a combination of formation properties, well spacing, and fracturing intensity (Zhang et al., 2019; Tong et al., 2024). For regions with different geological properties, how to specifically design well spacing and fracturing intensity is a key issue in improving the recovery factor of tight oil reservoirs. Geological parameters such as permeability, porosity, and oil saturation directly determine both the in-situ occurrence state and the producible potential of crude oil. For reservoirs with significant heterogeneity, using the same well spacing and fracturing intensity across different areas within the same block is unwise (Al-Fatlawi et al., 2019; Lei et al., 2020). It is essential to implement differential design based on a clear understanding of the reservoir properties (Xiong et al., 2018; Helmy et al., 2025). Fracturing intensity parameters such as proppant intensity and fluid intensity determine whether tight oil reservoirs can be effectively stimulated. In recent years, the well spacing for horizontal tight oil wells has been decreasing, leading to frequent inter-well fracture hits (Pankaj, 2018; Gupta et al., 2021; Fowler et al., 2022; Wang et al.,

* Corresponding author.
E-mail address: xiukunwang@cup.edu.cn (X.-K. Wang).
Peer review under the responsibility of China University of Petroleum (Beijing).

https://doi.org/10.1016/j.petsci.2026.04.017
1995-8226/

2024c). The matching relationship between well spacing and fracturing intensity warrants further investigation. Well spacing optimization needs to consider the direction and extent of fracture propagation, avoiding excessive density that leads to well interference, or too sparse spacing that results in insufficient reservoir drainage (Wang et al., 2024a, 2025c; Wu et al., 2025). Fracturing intensity optimization requires adjusting the fracture geometry based on well spacing, ensuring maximum Stimulation Reservoir Volume (SRV) while minimizing unnecessary fracture interference (Wang et al., 2026). In essence, well spacing and fracturing intensity are mutually constrained and interdependent (Tian et al., 2019; Xiong et al., 2020; Wang et al., 2024b). To achieve efficient development of tight oil reservoirs, it is essential to comprehensively consider the relationships between these two factors on a clear understanding of the reservoir geological properties.

Achieving collaborative optimization both well spacing and fracturing intensity is by no means an easy task. The influence of different factors on the long-term development performance of the reservoir is constrained by production time and therefore cannot be directly obtained through short-term field monitoring. Production prediction must instead rely on analytical or numerical simulation methods (Hu et al., 2017; Iqbal et al., 2023). Meanwhile, the recovery factor of tight oil reservoirs is affected by a multitude of factors, making it impractical to optimize all of them simultaneously (Guo et al., 2022; Hui et al., 2023; Rostamian et al., 2025). Since these factors have different degrees of influence on recovery factor, performing a full-factor experiment whether through analytical methods or numerical reservoir simulations would require an excessive number of runs, resulting in heavy computational workload and low efficiency.

To address these problems, this study proposes an integrated workflow that establishes a detailed geological model to characterize reservoir parameters, conducts fracture propagation simulations to define fracture features, performs main controlling factor analysis to identify the key influences on recovery factor, and utilizes numerical simulation to predict long-term production dynamics. Finally, based on response surface experiments, a collaborative optimization of the well spacing and fracturing intensity is achieved. The data used in this workflow are readily accessible from actual field, and only a small number of experimental samples are required. The optimization results are quantifiable and exhibit strong applicability. We implemented this workflow in an actual field case, identifying the optimal matching relationships among the reservoir, well spacing, and fracturing intensity, and established a predictive equation for recovery factor. Through data-driven main controlling factor analysis combined with numerical simulation, the approach effectively overcomes the limitations of practical field development and provides robust decision support for the efficient exploitation of tight oil reservoirs.

2. Analysis of factors affecting the production capacity of tight oil reservoirs

2.1. Applied machine learning methods and data processing

The Pearson correlation coefficient is widely used to measure linear relationships, and the Spearman rank correlation coefficient is used to evaluate monotonic relationships. However, data relationships in actual field are often more complex, and traditional methods have “blind spots” in capturing such patterns. To overcome this limitation, researchers have turned to information theory-based approaches, namely mutual information (MI). MI measures the statistical dependence between two random variables and is sensitive to any functional relationship. However, its calculation depends on the variable distributions and lacks a standardized range, making it difficult to compare results between different variable pairs. Moreover, for continuous variables, discretization is required, and the choice of discretization strategy greatly affects the results. The emergence of the Maximal Information Coefficient (MIC) method elegantly solves these problems. The MIC method calculates mutual information across all possible grid scales and normalizes the results to obtain a metric capable of capturing associations of any form between variables. In machine learning and data mining, the MIC method is commonly used to select features that are most strongly correlated with the target variable. The calculation process of the MIC mainly consists of three steps: data discretization and gridding, mutual information calculation, and determination of the maximal mutual information, as follows:

(1) Data discretization and gridding: divide the scatter plot formed by the data of variables X and Y into an $m \times n$ grid.
(2) Mutual information calculation: calculate the mutual information between the two discretized variables under different grid scales ($m \times n$), which can be expressed as follows:

$$\mathrm{MI}(X,Y)=\sum_{x\in X}\sum_{y\in Y}p(x,y)\log_2\frac{p(x,y)}{p(x)p(y)} \tag{1}$$

where $\mathrm{MI}(X,Y)$ is the mutual information between variables X and Y, $p(x)$ and $p(y)$ represent the marginal probability density functions of X and Y, and $p(x,y)$ is the joint probability density function of X and Y.

(3) Determination of the MIC: normalize the mutual information values obtained under different grid scales and then determine the maximum value:

$$\mathrm{MIC}(X,Y)=\max_{m\times n\leq B(N)}\frac{\mathrm{MI}[X,Y]}{\log_2(\min\{m,n\})} \tag{2}$$

where $\mathrm{MIC}(X,Y)$ is the maximal mutual information, $\log_2(\min\{m,n\})$ is the normalization term used for scaling the results, m and n represent the grid partition scales, $m\times n\leq B(N)$ is the constraint on the total number of grid cells, and B is typically set to the 0.6th power of the total sample size.

The dataset from actual field is typically large and may contain erroneous or invalid values. Therefore, data preprocessing is required before analysis. First, parameters unrelated to this study were removed, and wells with a large amount of missing data were excluded. Then, for wells with only minor data gaps, interpolation was used to fill in the missing values. Finally, outlier detection was performed on the reservoir geological and engineering parameters using the boxplot method and outlier monitoring, and the detected outliers were eliminated. The ranges of the processed data are shown in Table 1.

Table 1
Parameter ranges following data preprocessing.

Parameters	Value	Parameters	Value
Porosity, %	5.1–12	Effective pay encounter rate, %	50–80
Permeability, mD	0.1–4.6	Effective thickness, m	2–20
Oil saturation, %	35–70	Proppant intensity, m^3/m	3–26
Reservoir abundance	0.2–3	Fracturing fluid intensity, m^3/m	160–560
Fracture height, m	5–40	Stable water cut, %	35–100

2.2. Analysis of key factors controlling productivity

Optimization work is usually carried out before large-scale field development, when the production time of the block is relatively short. Since tight oil production declines rapidly, the early production characteristics are distinct and show a strong correlation with the Estimated Ultimate Recovery (EUR). Therefore, using the cumulative oil production in the first year as an indicator to characterize well productivity is reasonable. The MIC method is used to analyze and rank the influence of geological and engineering parameters on the cumulative oil production of horizontal wells during the first year, as shown in Fig. 1. Among all parameters, the stable water cut has the greatest impact on first-year cumulative oil production, followed by porosity, proppant intensity, permeability, and fluid intensity. Porosity reflects the reservoir storage capacity, and permeability determines the ease of oil-water flow in the matrix and the diffusion of fracturing fluid. Fluid intensity and proppant intensity determine the overall scale of hydraulic fracturing.

The results of the MIC analysis indicate that the stable water cut is the most influential factor affecting the initial productivity of fractured horizontal wells. The water cut is a complex function of geological parameters (such as porosity and permeability) and fracturing parameters (such as proppant intensity and fluid intensity). Accurate matching of water cut in numerical simulations is therefore essential. The fracturing fluid retained due to the closure of unpropped fractures leads to a redistribution of formation fluids. If the original reservoir properties are used for calculation, substantial errors may arise in both history matching and production prediction. Hence, reconstructing the saturation field is crucial which is an important aspect often overlooked in previous studies.

A large amount of retained fracturing fluid alters the distribution of oil, water, and energy in the reservoir, causing tight oil or shale oil reservoirs to exhibit different oil and water production dynamics compared to conventional reservoirs. Male (2019) summarized the water cut variation over time for thousands of shale oil wells in the major U.S. shale oil producing regions of Bakken, Eagle Ford, and Permian. Despite significant differences in water cut across individual shale oil wells, the overall trend follows an L-shaped curve, where the water cut decreases rapidly at first, then flattens out within 6 to 12 months. Guan et al. (2024) conducted a study on a continental shale oil block in the Bohai Bay Basin, China. The results showed that the initial water cut was high but decreased rapidly, reaching a plateau value after approximately six months, and then remained relatively stable. Fig. 2 presents a box plot of the water cut variation over time for all wells

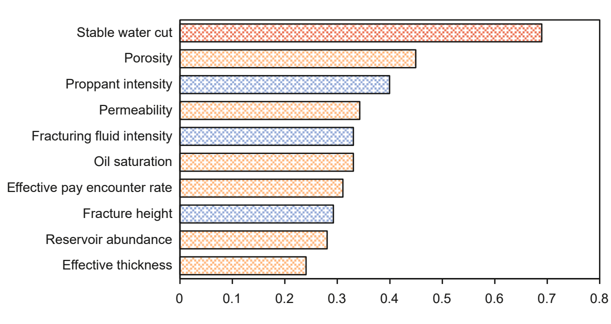

Fig. 1. Ranking of factors according to their impact on first-year cumulative oil production.

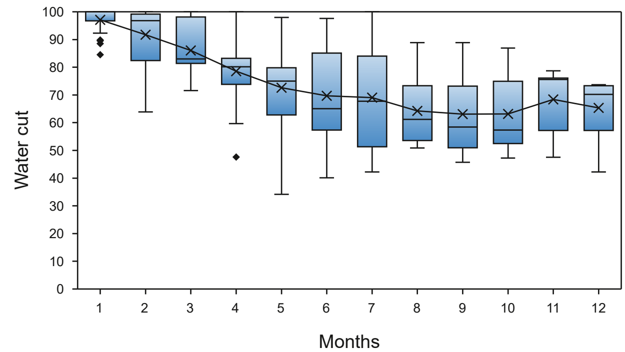

Fig. 2. Variation of water cut over production time.

in this study block, demonstrating a consistent trend, which is similar to that of U.S. shale/tight oil.

When the fracturing intensity is similar, the stable water cut shows a strong correlation with well productivity. Guan et al. (2024) found that the cumulative oil production in the first year of multi-stage fractured horizontal wells is strongly correlated with stable water cut. The lower the stable water cut, the higher the cumulative oil production in the first year. Furthermore, the first-year cumulative oil production is strongly positively correlated with the predicted estimated ultimate recovery (EUR), indicating that stable water cut also influences long-term productivity. Male et al. (2018) analyzed production data from tens of thousands of wells in the Bakken shale oil block. The results showed that water cut is the most important factor influencing the EUR of fractured horizontal wells. The level of stable water cut reflects the effectiveness of reservoir stimulation and serves as effective evidence for the retention of fracturing fluid in the formation.

3. Integrated workflow for multi-fractured horizontal wells in tight oil reservoirs

In the preceding analysis, we employed a simple machine-learning algorithm to identify the dominant controlling factors affecting the productivity of tight-oil wells. To achieve the optimal matching relationships among the reservoir, well spacing, and fracturing intensity, we developed an integrated workflow which consists of three modules: refined modeling, numerical simulation, and collaborative optimization, as illustrated in Fig. 3.

Modeling is based on field-monitored data to establish a three-dimensional fine-scale geological model and a geo-mechanical model of the reservoir. The geological model represents the spatial distribution of reservoir properties and serves as the foundation for subsequent studies, while the geo-mechanical model reflects the mechanical characteristics of the reservoir, determining the difficulty of hydraulic fracture propagation. Numerical simulation involves conducting both fracture propagation simulation and reservoir simulation. Based on clearly defined reservoir geological and mechanical parameters, fracture propagation simulations are performed for single wells under different fracturing designs corresponding to various reservoir properties. The simulation results are then seamlessly integrated into a high-performance simulator to perform reservoir numerical simulation, enabling the identification of production dynamics under different well pattern parameters. Collaborative optimization, in turn, uses the dominant factors as variables and the recovery factor of tight oil wells as the objective function, optimizing the well spacing and fracture intensity parameters under different reservoir conditions to achieve optimal matching. This integrated workflow is not

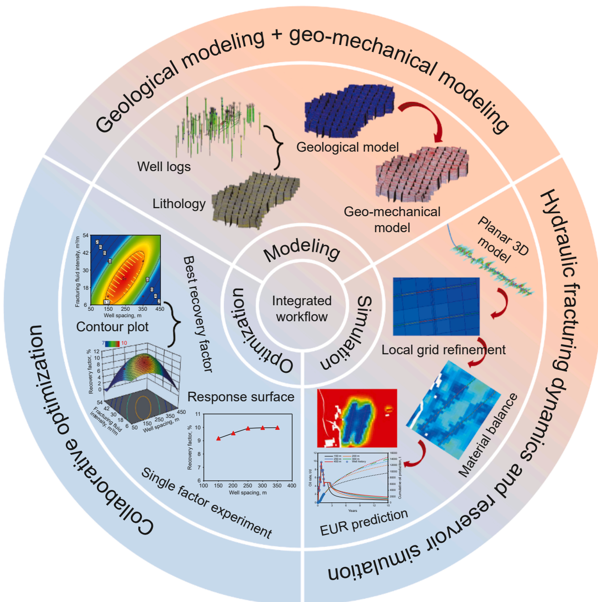

Fig. 3. Integrated workflow for collaborative optimization of tight oil reservoir development.

constrained by long-term production data; it utilizes only routine field test results and short-term production data to perform optimization. It is simple, efficient, and highly applicable to field engineering practice.

3.1. Geological and geomechanical modeling

Three-dimensional geological modeling employs data from well logging, seismic, and core sampling and so on. These data are typically obtained during the early stages of development like geological exploration or drilling and are often easy to collect and acquire, serving as essential information for understanding reservoir characteristics. By interpreting well logs and conducting geological stratification for individual wells, combined with seismic data and core sampling results, the reservoir's structural and lithology models are established. Subsequently, a lithofacies-constrained stochastic modeling method is applied to generate property models, including parameters such as porosity and permeability. By applying lithology constraints, the issue of invalid reservoirs such as interlayers being interpolated into effective reservoirs during the modeling process is avoided. This approach reduces the uncertainty of stochastic simulations and ensures that the reservoir properties better conform to reservoir formation mechanism and sedimentary characteristics. Fig. 4(a) presents the permeability model of the study area, and Table 2 lists the values and ranges of various properties in the geological model.

The three-dimensional geo-mechanical model is primarily constructed using basic data such as compressional wave time, shear wave time, and density logs. Based on geo-mechanical calculation formulas, data around well locations are first computed, and then a stochastic modeling method is applied to extend the results across the entire study area. Based on the geological model, three-dimensional geo-mechanical properties such as Poisson's ratio, Young's modulus, maximum horizontal principal stress, and minimum horizontal principal stress are established for the study area to support subsequent fracture propagation simulations. Fig. 4(b) illustrates the minimum horizontal principal stress model of the study area, and Table 3 presents the values and ranges of the geo-mechanical model properties.

3.2. Hydraulic fracturing dynamics simulation

Based on the actual well locations, trajectories, and logging data from the field, a dynamic fracture propagation simulation model is established. The geological and mechanical parameters, as well as formation undulations, are calibrated using the geo-mechanical model developed in the previous section. Incorporating completion data and pumping schedules, the dynamic fracture propagation is simulated using a fully coupled, grid-oriented iterative scheme. The simulation sequence at each time step begins with the calculation of the net pressure:

$$P_{\mathrm{net}} = P_{\mathrm{f}} - \sigma - P_{\mathrm{p}} \tag{3}$$

where P_{net} is the net pressure, MPa; P_{f} is the fluid pressure inside the fracture, MPa; σ is the minimum horizontal principal stress, MPa; and P_{p} is the pore pressure, MPa. Subsequently, the fracture width is solved. As shown in Fig. 5, a shear-slip model is employed to decouple rock deformation by integrating the net pressure within a defined shear dampening radius:

$$w(x,y) = \frac{2(1-\nu^2)}{\pi E} \iint_{\Omega_{S_{\mathrm{d}}}} \frac{P_{\mathrm{net}}(x',y')}{\sqrt{(x-x')^2 + (y-y')^2}} \mathrm{d}x' \mathrm{d}y' \tag{4}$$

where w is the fracture width, m; ν is Poisson's ratio; E is Young's modulus, GPa; and $\Omega_{S_{\mathrm{d}}}$ represents the integration domain restricted by the shear dampening radius S_{d}, which accounts for interfacial slippage. For tight oil reservoirs, where geological conditions are complex, interlayers are well developed, and strong

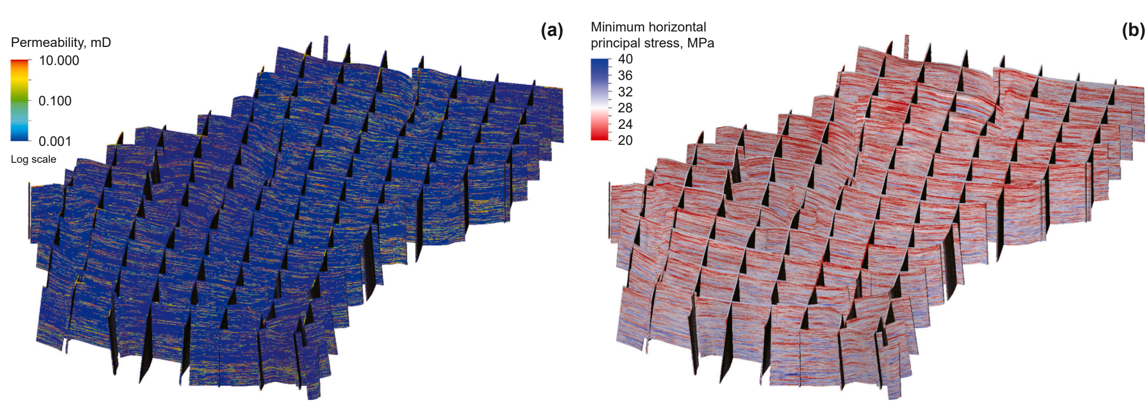

Fig. 4. Raster map and property distribution. **(a)** Permeability model. **(b)** Minimum horizontal principal stress model.

Table 2
Geological model properties and their ranges.

Property	Range	Average value
Porosity, %	8–13	10.2
Permeability, mD	0.1–10.3	0.35
Oil saturation, %	35–70	48

Table 3
Geomechanical model properties and their ranges.

Property	Range	Average value
Poisson's ratio	0.23–0.24	0.236
Young's modulus, GPa	20–36	30.6
Minimum horizontal principal stress, MPa	20–40	28.3
Maximum horizontal principal stress, MPa	25–45	36.8

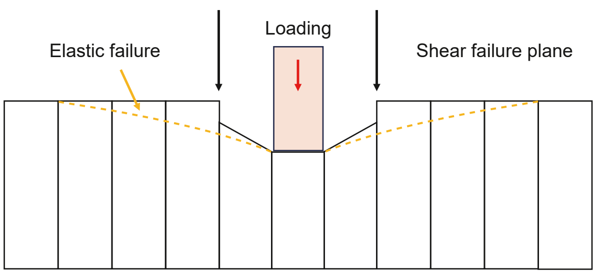

Fig. 5. Shear slip displacement model (dashed line for linear elastic model).

anisotropy exists, shear failure exerts a greater influence, making the shear-slip model more suitable. With the fracture geometry defined, the fluid pressure distribution is solved by satisfying the mass conservation equation:

$$\frac{\partial w}{\partial t}+\nabla\cdot\vec{q}+q_{\text{leak}}-q_{\text{inj}}=0 \tag{5}$$

where q is the velocity vector of fracturing fluid, m^3/d; q_{leak} is the liquid leak-off rate, m^3/d; and q_{inj} is the injection rate, m^3/d. The flow rate q is governed by Poiseuille's law, where the updated fluid pressure then triggers a recalculation of the net pressure and fracture width until convergence. Parameters including fracture length and height are dynamically calculated throughout the process. The reliability of the fracture simulation is further enhanced through history matching of the pumping schedule. During the fracture propagation simulation, factors such as fracturing fluid leak-off, proppant transport, and stress shadow effects caused by fracture interference are taken into account. The stress shadow effect can be calculated:

$$\sigma_{\text{ss}}=\frac{1.057\cdot P_{\text{net}}}{0.3048^{t}\cdot D^{t}} \tag{6}$$

where σ_{ss} is the stress shadow, MPa; D is the distance from the fracture face, m; and t is transverse exponent that controls stress decay. The value of the exponent is 2 or less, with smaller values being more suitable for low-permeability reservoirs.

In traditional approaches, fracture toughness is determined in the laboratory and is difficult to upscale to the field scale. In contrast, the process zone stress (PZS) can be measured and calibrated during field operations:

$$\text{PZS}=P_{\text{ISIP}}-P_{\text{c}} \tag{7}$$

where PZS is the process zone stress, MPa; P_{ISIP} is the instantaneous shut-in pressure, MPa; and P_{c} is the closure pressure, MPa. The fracture propagation is evaluated using the PZS criterion:

$$P_{\text{net}}>(1-\varepsilon)\cdot\text{PZS} \tag{8}$$

where ε is the fracture criteria tolerance. This criterion overcomes the stress singularity problem inherent in conventional linear elastic models, making it more consistent with actual field conditions and resulting in more accurate predictions of fracture length. Fig. 6 illustrates the distribution of effective fracture conductivity in a horizontal well within the study area after hydraulic fracturing. To ensure that the fracture model reflects realistic field operating conditions, the fracturing model parameters are set based on actual field completion and pumping data, and the simulated pressure is calibrated to match the measured field pumping pressure, as shown in Fig. 7. In practice, fracture propagation dynamics are influenced by multiple factors, including reservoir heterogeneity, the degree of natural-fracture development, fracturing fluid type, and pumping parameters (Wang et al., 2025a, 2025b; Garcia et al., 2025; Nolte et al., 2025). This fracture model provides reliable estimation of key fracture parameters and is suitable for guiding field-scale reservoir simulation and development decisions. Its applicability to more complex fracture

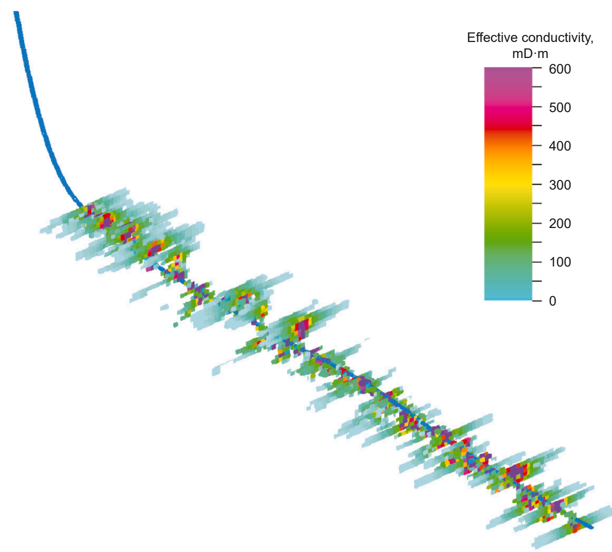

Fig. 6. Fracture effective conductivity, mD·m.

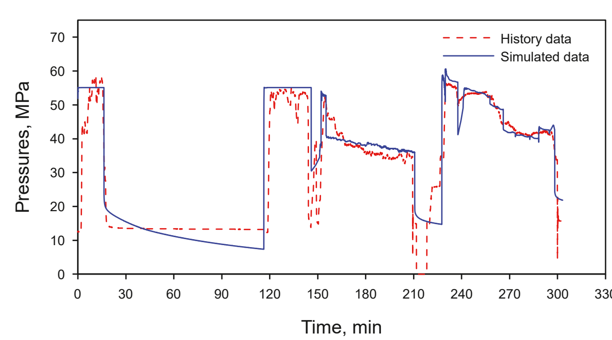

Fig. 7. Pumping pressure matching. The dashed line represents actual pressure, while the solid line represents simulated pressure.

behaviors, such as reorientation, branching, and strong fracture interaction, still requires further verification.

3.3. Saturation field reconstruction and reservoir simulation

3D geological modeling and fracture simulation are employed to define reservoir properties and fracture geometries, respectively, providing the basis for the reservoir numerical simulation. The results of geological modeling and fracture propagation simulation are seamlessly integrated into a high-performance reservoir simulator. The simulator adopts a black oil model governed by the mass conservation law. For the phase l ($l = \mathrm{o}$ for oil, $l = \mathrm{w}$ for water), the continuous partial differential equation describing multi-phase flow in porous media is defined as:

$$\nabla\cdot\left[\frac{\mathbf{k}k_{\mathrm{r}l}}{\mu_l B_l}\left(\nabla p_l - \gamma_l \nabla Z\right)\right] + q_{l,\mathrm{sc}} = \frac{\partial}{\partial t}\left(\frac{\phi S_l}{B_l}\right) \tag{9}$$

where $\mathbf{k}$ is the absolute permeability tensor; $k_{\mathrm{r}l}$ is the relative permeability of the oil or water phase; μ_l is the viscosity, mPa·s; B_l is formation volume factor; p_l is the phase pressure, MPa; γ_l is the specific weight; Z is the depth, m; $q_{l,\mathrm{sc}}$ represents the source/sink term per unit volume; ϕ is the porosity; and S_l is the saturation. To solve this nonlinear system numerically, the control volume finite difference method is employed using a fully implicit scheme.

$$\begin{aligned}&\sum_{j\in N_i} T_{ij}^{n+1}\lambda_{l,ij}^{n+1}\left(p_j^{n+1} - p_i^{n+1} - \gamma_{ij}^{n+1}\Delta Z_{ij}\right) + Q_i^{n+1}\\ &\quad = \frac{V_i}{\Delta t}\left[\left(\frac{\phi S_l}{B_l}\right)_i^{n+1} - \left(\frac{\phi S_l}{B_l}\right)_i^{n}\right]\end{aligned} \tag{10}$$

where N_i is the set of neighboring grid blocks connected to block i; superscripts n and $n+1$ represent the current and next time steps; $\lambda_{l,ij}$ is the mobility term of the oil phase at the interface; Q_i is the well production rate for block i; V_i is the grid block volume; and Δt is the time step size. The fluid flow between adjacent grid blocks depends on the transmissibility:

$$T_{ij} = \beta \frac{A_{ij}}{d_i + d_j}\cdot\frac{k_i k_j\left(d_i + d_j\right)}{k_i d_j + k_j d_i} \tag{11}$$

where β is a geometric factor; A_{ij} is the interface area, m^2; d_i and d_j are distances from the grid centers to the interface, m; and k_i, k_j are the permeabilities of adjacent blocks, mD. Regarding the fracture representation, a Local Grid Refinement (LGR) method is employed, as shown in Fig. 8. To address the scale disparity between physical fractures and simulation grids, an equivalent permeability approach is applied. The effective permeability of the LGR blocks is derived as:

$$k_{\mathrm{eff}} = \frac{k_{\mathrm{f}}\cdot w_{\mathrm{f}}}{w_{\mathrm{LGR}}} \tag{12}$$

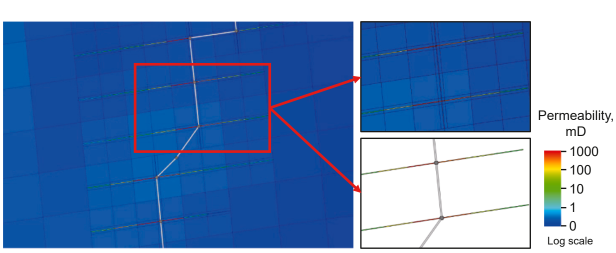

Fig. 8. Local grid refinement method.

where k_{eff} is the effective permeability, mD; w_{f} is the width of the hydraulic fracture, m; and w_{LGR} is the width of the refined grid block, m. The resulting Jacobian matrix is solved via the Newton-Raphson method to update pressure and saturation fields at each time step. The model setup uses fluid PVT parameters and relative permeability data obtained from laboratory tests, along with field-specific data such as completion, perforation, and well operating conditions. All the aforementioned numerical computations and the solution of the governing equations were performed using the CMG-IMEX reservoir simulator.

A large volume of fracturing fluid is injected into the formation under high pressure during hydraulic fracturing process. However, only a small portion of the fluid is recovered, while a significant amount remains trapped, resulting in a two-phase oil-water flow within the reservoir (Edwards et al., 2017; Cai and Dahi Taleghani, 2019; Yang et al., 2019). Sharma and Manchanda (2015) suggested that during the hydraulic fracturing process, a large number of secondary fractures are generated, with over 90% of the fracturing fluid entering these unpropped fractures. The fracture system in tight oil reservoirs after hydraulic fracturing is complex, primarily consisting of natural fractures and induced fractures. Natural fractures are mainly structural fractures and bedding fractures, while induced fractures are primarily hydraulic fractures and shear fractures caused by induced stress. Hydraulic fracturing field tests in the United States have involved coring and imaging logging of horizontal wells after fracturing. The results indicated that no complex fracture network was found in the formation. Instead, near the main fractures, a large number of micro-scale fractures parallel to the main fractures were observed and their quantity far exceeded the number of designed clusters (Raterman et al., 2018; Fu et al., 2021). In recent years, hydraulic fracturing field tests in China's Ordos Basin and Junggar Basin have similarly fracture swarms, and the proppant migration distance within the fractures is limited. Due to low permeability of the matrix and the short injection time, very little fracturing fluid can leak off into the matrix, with the fracturing fluid mainly remaining in the primary and secondary fractures (Wang and Leung, 2015; Zhang et al., 2021). In the fracture swarms, secondary fractures dominate in number. However, these fractures contain only a small amount of proppant near the wellbore, and the conductivity in these regions is higher than in the matrix. Fracturing fluid is preferentially produced from the regions with higher conductivity. During the flowback stage, the bottom-hole pressure continuously decreases. Under the overburden stress, the secondary fractures quickly close due to the lack of proppant locking a significant amount of fracturing fluid within the reservoir (Sharma and Manchanda, 2015; Wu et al., 2017; Wu and Sharma, 2017). In previous studies, we find that fracturing fluid is easily produced from high-conductivity regions within the fracture swarms, while it is difficult to produce from low-conductivity regions. The difference in conductivity creates varying pressure gradients during the flowback process. The pressure gradient formed between the high-conductivity regions in the fractures and the matrix causes fracturing fluid originally flowing toward the wellbore in the low-conductivity regions to reverse direction and migrate into the matrix, leading to the retention of fracturing fluid within the reservoir (Wang et al., 2025d).

Field cases shows that the fracturing fluid flow-back ratio in tight oil reservoirs is low, typically ranging from 10% to 30% (Alkouh and Wattenbarger, 2013; Abualfaraj et al., 2014). The lower the flow-back ratio, the higher the subsequent productivity and the lower the water cut. Fig. 9 illustrates our hypothesis of SRV and fracturing fluid distribution after hydraulic fracturing for high-yield and low-yield wells. Under the same fracturing intensity, wells with higher productivity typically have a larger SRV, with

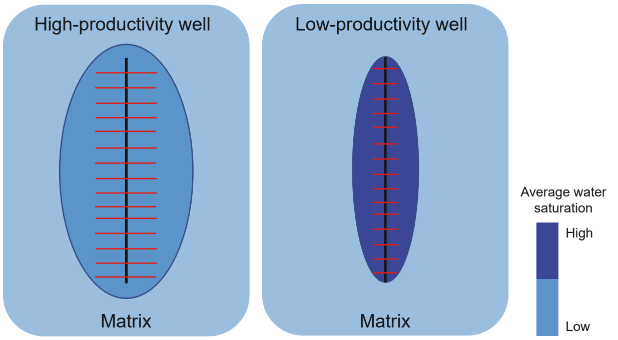

Fig. 9. Schematic diagram of fracturing fluid invasion region and average water saturation for wells with different productivity levels. The ellipses indicate the region of fracturing-fluid invasion, i.e., SRV.

fracturing fluid spreading farther and penetrating a larger area. The average water saturation within SRV is lower, resulting in a lower flowback rate during flowback and a lower water cut during production. In contrast, wells with lower productivity have a limited SRV, with fracturing fluid accumulating near the wellbore, penetrating a smaller area. The average water saturation within the stimulated area is higher, leading to a higher flow-back ratio and a higher water cut.

As shown in Fig. 10, we use the material balance (MB) method for fracturing fluid to calculate the changes in reservoir properties after fracturing fluid injection. The volume of fracturing fluid pumped for each well and the fracture-controlled area are statistically analyzed. Based on the principle of material balance, the original oil saturation and porosity are modified and corrected, quickly restoring the oil-water distribution in the formation after large-scale multi-stage hydraulic fracturing of horizontal wells.

According to the principle of material balance,

$$V_{\phi\mathrm{post}} = V_{\phi\mathrm{pre}} + V_{\mathrm{ff}} \tag{13}$$

where $V_{\phi\mathrm{post}}$ is the post-fracturing pore volume, m^3; $V_{\phi\mathrm{pre}}$ is the pre-fracturing pore volume, m^3; and V_{ff} is the fracturing fluid volume, m^3. The pore volume multiplier can then be calculated as,

$$\mathrm{Mul}_{\phi} = \frac{\phi_{\mathrm{post}}}{\phi_{\mathrm{pre}}} = \frac{V_{\phi\mathrm{post}}}{V_{\phi\mathrm{pre}}} \tag{14}$$

where Mul_{ϕ} is the pore volume multiplier, ϕ_{post} is the post-fracturing porosity, and ϕ_{pre} is the pre-fracturing porosity. The water saturation and oil saturation multipliers can be calculated using the following formula,

$$\mathrm{Mul}_{S_{\mathrm{w}}} = \frac{S_{\mathrm{wpost}}}{S_{\mathrm{wpre}}} = \frac{S_{\mathrm{wpre}} \times V_{\phi\mathrm{pre}} + V_{\mathrm{ff}}}{V_{\phi\mathrm{post}}} \tag{15}$$

$$\mathrm{Mul}_{S_{\mathrm{o}}} = \frac{1 - S_{\mathrm{wpost}}}{S_{\mathrm{opre}}} \tag{16}$$

where $\mathrm{Mul}_{S_{\mathrm{w}}}$ and $\mathrm{Mul}_{S_{\mathrm{o}}}$ are the water saturation multiplier and oil saturation multiplier, S_{wpre} and S_{wpost} are the water saturation before and after fracturing, respectively, and S_{opre} is the oil saturation before fracturing.

Subsequently, the long-term production dynamics of the block are predicted using a high-performance reservoir numerical simulator. Fig. 11 shows the pressure propagation over 15 years of production for two wells at different well spacings. At a well spacing of 400 m, no pressure interference occurs between wells, resulting in high remaining pressure and the presence of remaining oil. As the well spacing decreases, pressure interference between wells gradually increases, and the interference becomes more severe as the well spacing reduces further.

Fig. 12 illustrates the cumulative oil production and oil production rate curves over 15 years for a well at different well spacings within the block. The EUR decreases as the well spacing decreases, with a more significant decline in EUR once the well spacing drops below 250 m. When the well spacing is 150 m, the EUR is reduced by 34.7% compared to the current well spacing. Fig. 13 presents the box plot of EUR over 15 years for all wells in the block at different well spacings. When the well spacing is 250 m, the EUR loss is approximately 13% compared to the initial well spacing. With minimal pressure interference between wells and a high degree of well utilization, a 250-m spacing is considered the optimal development spacing. This value will guide the design of subsequent experiments.

4. Collaborative optimization of well spacing and fracturing intensity

The tight oil reservoir has poor formation permeability, and to achieve an extended stable high-production period and improve

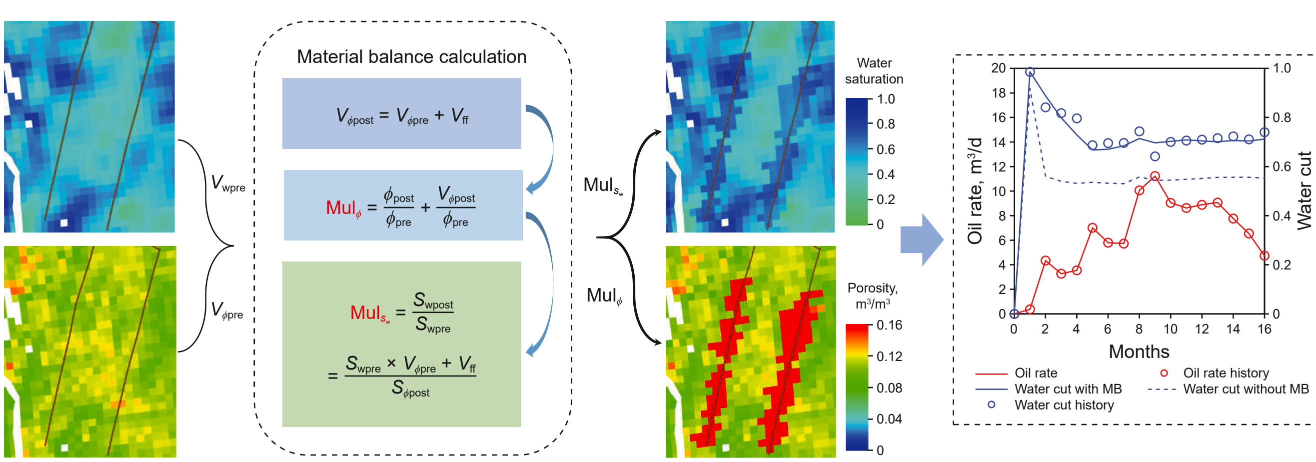

Fig. 10. Material balance (MB) calculation process.

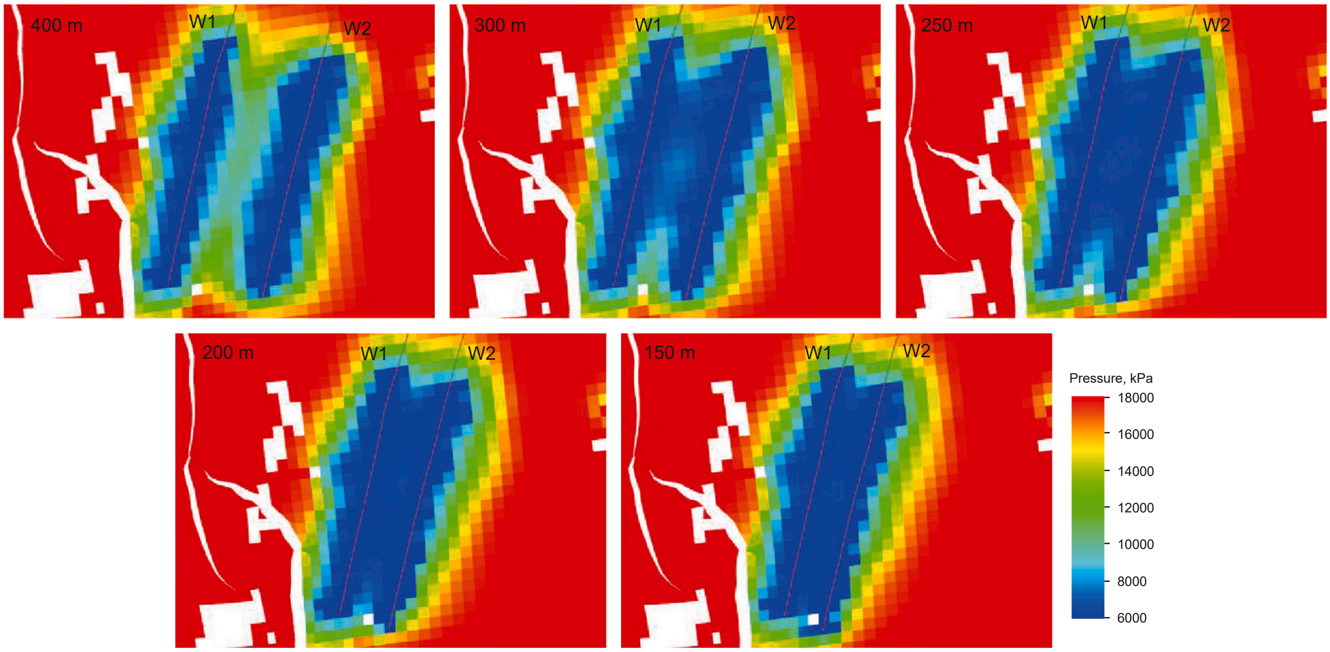

Fig. 11. Pressure propagation under different well spacings.

reservoir utilization through large-scale fracturing of horizontal wells, it is essential to understand the impact of key factors such as reservoir geological properties, well pattern, and fracture network matching. In the above study, we identified the main factors influencing productivity as the average reservoir permeability, well spacing, and fracturing intensity. Therefore, in this section, we specifically establish a reservoir-well spacing-fracture network collaborative optimization method for the target block, aiming to maximize recovery factor and improve reservoir utilization, and conduct matching study. Two wells from the same layer within the block are selected for the study. Based on the reservoir-well spacing-fracture network collaborative optimization method, a single-factor experiment is first conducted. Fracture propagation simulation and reservoir numerical simulation are performed for different experiments to analyze the impact of well spacing, fracturing intensity, and reservoir permeability on recovery factor. Building on the results of the single-factor experiments, a multi-factor response surface experiment is then conducted to clarify the interactions between the parameters and provide adjustment strategies, offering guidance for subsequent development.

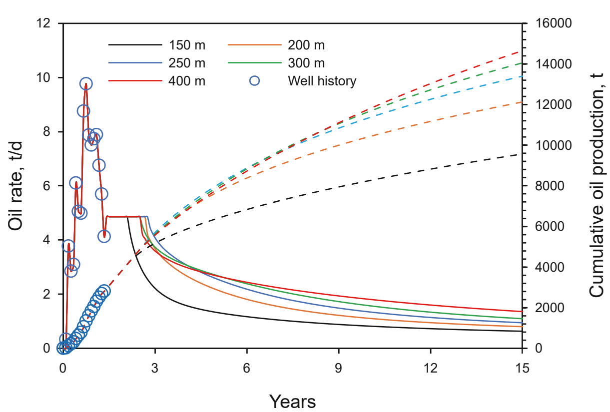

Fig. 12. Oil production rate and cumulative oil production at different well spacings.

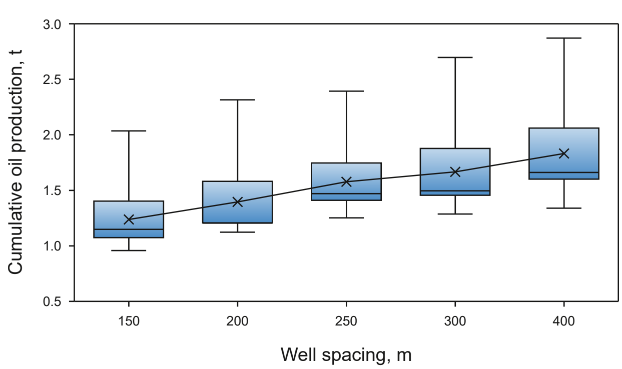

Fig. 13. Box plot of predicted 15-years EUR under different well spacings.

4.1. Single factor experiment

A single-factor experiment involves changing one factor at a time while keeping the other factors constant to observe the independent effect of that factor on the target outcome. In this study, the recovery factor over 15 years of production is used as the evaluation index. Each factor is designed with five levels: well spacing ranges from 150 m to 350 m, fracturing fluid intensity ranges from 12 m^3/m to 36 m^3/m, and the average reservoir permeability ranges from 0.1 mD to 0.5 mD. The fixed conditions (current situation) are as follows: horizontal well spacing of 250 m, fracturing fluid intensity of 24 m^3/m, and average permeability of 0.3 mD. The study investigates the impact of these parameters on the recovery factor of horizontal wells. The experimental design is shown in Table 4.

Fig. 14 presents the results of the single-factor experiment. As shown in Fig. 14(a), with increasing well spacing, the recovery factor of horizontal wells gradually rises, but the rate of increase diminishes. When the well spacing is small, well spacing is the primary factor influencing the recovery factor and under the current fracturing intensity, severe well interference occurs. Although the controlled reservoir volume is low, the drop in production caused by pressure interference is more significant, leading to a

Table 4
Single factor experimental design.

Experiment number	Well spacing, m	Fracturing fluid intensity, m^3/m	Average permeability, mD
1	150	12	0.1
2	200	18	0.2
3	250	24	0.3
4	300	30	0.4
5	350	36	0.5

lower recovery factor. As the well spacing increases, fracturing intensity becomes the dominant factor affecting the recovery factor. Since the fracturing intensity is limited, increasing the well spacing results in only a small increase in controlled reservoir volume. However, it somewhat mitigates or reduces well interference, leading to an increase in production, and thus, the recovery factor rises, though the increase is smaller.

As shown in Fig. 14(b), under the current well spacing and permeability conditions, reducing the fracturing intensity results in a decrease in hydraulic fracture length, leading to a reduction in the reservoir stimulation volume. This decreases the inter-well permeability, which in turn causes a lower recovery factor. Conversely, increasing the fracturing intensity helps to extend the fractures, but as the fractures approach or connect, well interference intensifies, leading to a decline in production and a subsequent decrease in the recovery factor.

As shown in Fig. 14(c), under the current engineering conditions, a decrease in permeability leads to a decline in reservoir permeability, reducing the flow capacity of the reservoir, which in turn lowers horizontal well production and recovery factor. Conversely, an increase in permeability enhances the reservoir's flow capacity, causing pressure propagation to occur more rapidly. However, this intensifies well interference, resulting in a moderate decrease in production and a subsequent reduction in recovery factor. The well spacing, fracturing intensity, and reservoir permeability all influence horizontal well production and controlled reservoir volume, which in turn affect the recovery factor. Therefore, further analysis of the interactions between these parameters is necessary.

4.2. Response surface methodology

To better clarify the reservoir-well spacing-fracture network match of the study block, a response surface methodology (RSM) experiment is conducted with horizontal well spacing, fracturing intensity, and reservoir permeability as the response variables. The independent variables are detailed in Table 5. When considering the fracturing intensity, we keep the sand ratio constant and vary the fracturing fluid intensity. The objective is to optimize the recovery factor of the tight oil reservoir. The model is a three-factor, three-level design using the Box-Behnken experimental design, requiring 17 experiments in total. The 15-years recovery factors under different conditions are calculated based on reservoir numerical simulation, as shown in Table 6.

Subsequently, perform multiple regression analysis on the experimental results using the Quadratic method for fitting, the regression equation in terms of coded factors is expressed as follows:

$$R = 9.93 - 0.1225A + 0.0875B + 0.2300C + 1.12AB$$
$$+0.8125AC + 0.1925BC - 0.9763A^2 - 0.5062B^2 - 0.5213C^2 \tag{17}$$

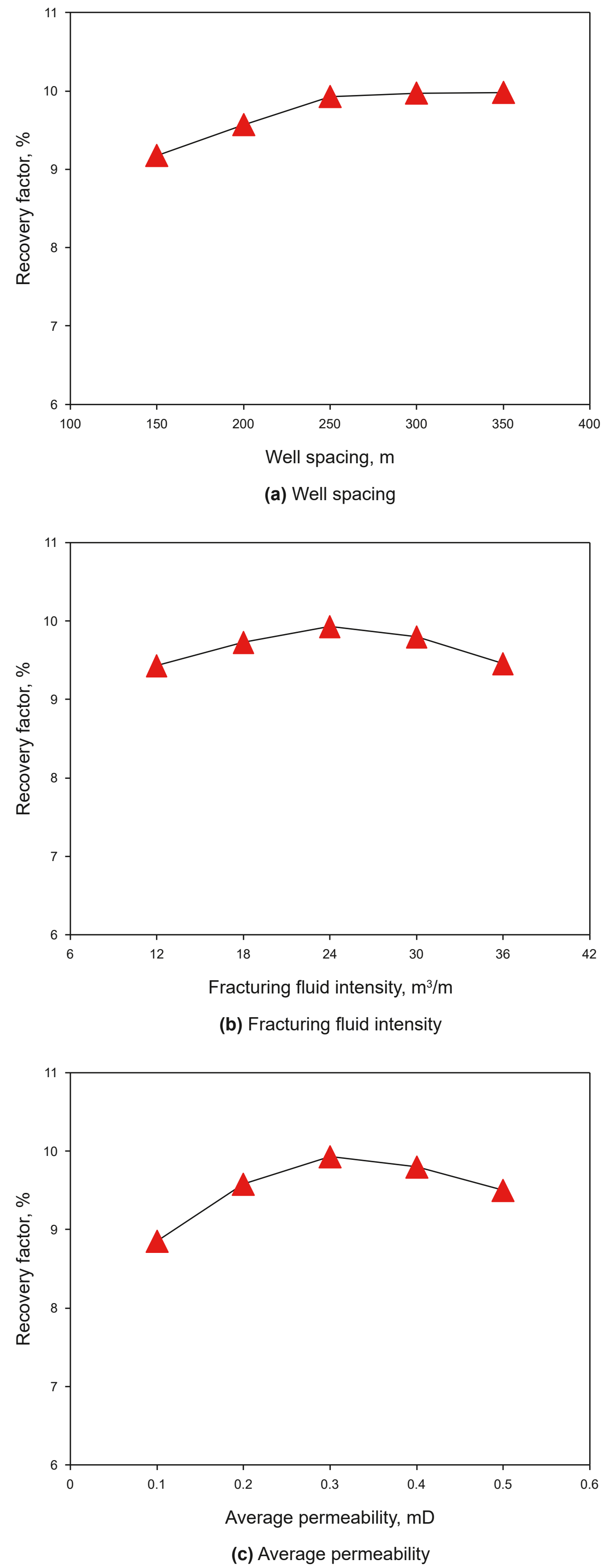

Fig. 14. Effect of different parameters on recovery factor.

where R is the recovery factor; A, B, and C are the coded variables corresponding to the actual factors W (well spacing), F (fracturing fluid intensity), and P (average reservoir permeability), respectively. In the coded space, −1, 0, and +1 represent the low, center,

Table 5
Factors and levels for RSM design.

Level	Well spacing W, m	Fracturing fluid intensity F, m^3/m	Average permeability P, mD
−1	150	12	0.1
0	250	24	0.3
1	350	36	0.5

Table 6
Experimental design and results of co-optimization.

Experiment number	Experiment plan			Experiment code			Results
	W, m	F, m^3/m	P, mD	A	B	C	R, %
1	250	12	0.1	0	−1	−1	9.03
2	250	36	0.1	0	1	−1	8.55
3	350	24	0.5	1	0	1	9.45
4	150	12	0.3	−1	−1	0	9.45
5	250	24	0.3	0	0	0	9.93
6	250	24	0.3	0	0	0	9.93
7	150	24	0.1	−1	0	−1	9.04
8	250	12	0.5	0	−1	1	8.87
9	250	24	0.3	0	0	0	9.93
10	150	36	0.3	−1	1	0	7.65
11	250	36	0.5	0	1	1	9.16
12	350	24	0.1	1	0	−1	7.13
13	250	24	0.3	0	0	0	9.93
14	250	24	0.3	0	0	0	9.93
15	150	24	0.5	−1	0	1	8.11
16	350	12	0.3	1	−1	0	7.00
17	350	36	0.3	1	0	0	9.69

and high levels of each factor. The coded model is used to evaluate the relative significance of factors and their interactions. The actual recovery factor prediction equation is as follows:

$$\begin{aligned} R = {} & 9.65375 + 0.012950W - 0.0818750F - 3.11250P \\ & + 0.0009354WF + 0.040625WP + 0.0802083FP \\ & - 0.000098W^2 - 0.00351563F^2 - 13.03125P^2 \end{aligned} \tag{18}$$

where R is the recovery factor; W is the horizontal well spacing, m; F is the fracturing fluid intensity, m^3/m; and P is the average permeability of the reservoir, mD. This equation enables the direct input of actual field data to forecast the recovery factor.

4.3. Analysis of variance (ANOVA)

Table 7 presents the results of the analysis of variance for the response surface experiment. Generally, a P-value less than 0.05 is considered significant, while a P-value less than 0.001 indicates a highly significant effect. The F-value of the collaborative optimization regression model is 45.87, with a P-value less than 0.0001, and the model's coefficient of determination $R^2 = 0.9833$, $R^2_{adj} = 0.9619$, indicating that the established quadratic equation has high significance. This model can effectively reflect the relationship between the factors and recovery factor. Fig. 15 presents the comparison between the predicted recovery factors and the corresponding simulation results and the predicted coefficient of determination $R^2_{pred} = 0.7332$. It is calculated based on the predicted residual error sum of squares statistic, using a leave-one-out cross-validation procedure in which each data point is removed in turn and predicted using a model built from the remaining data. This model has a certain predictive capability within the studied design space. The coefficient of variation (C.V.) is 2.14%, which is less than 5%, demonstrating good repeatability of the experimental model. The equation exhibits good precision and reliability, making it suitable for theoretical prediction in reservoir-well spacing-fracture network collaborative optimization experiments. By comparing the F-values of each factor in the regression equation, it is evident that the order of influence on the recovery factor is: average reservoir permeability > horizontal

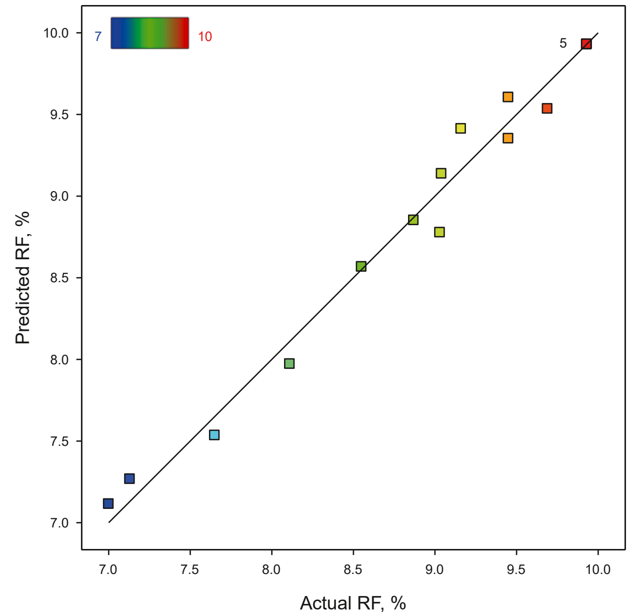

Fig. 15. Correlation between actual and predicted values of recovery factor.

Table 7
Response surface regression model analysis of variance.

Source	Sum of squares	Degrees of freedom	Mean square	F-value	P-value	Significance
Model	15.3	9	1.7	45.87	<0.0001	***
A	0.12	1	0.12	3.24	0.1149	
B	0.0612	1	0.0612	1.65	0.2395	
C	0.4232	1	0.4232	11.42	0.0118	*
AB	5.04	1	5.04	135.98	<0.0001	***
AC	2.64	1	2.64	71.24	<0.0001	***
BC	0.1482	1	0.1482	4	0.0856	
A^2	4.01	1	4.01	108.27	<0.0001	***
B^2	1.08	1	1.08	29.11	0.001	**
C^2	1.14	1	1.14	30.87	0.0009	***
Residual	0.2594	7	0.0371			
R^2	0.9833	R^2_{adj}	0.9619	C.V.%	2.14	

Notes: P-value < 0.05 indicates statistical significance (*), P-value < 0.01 indicates moderate statistical significance (**), and P-value < 0.001 indicates high statistical significance (***).

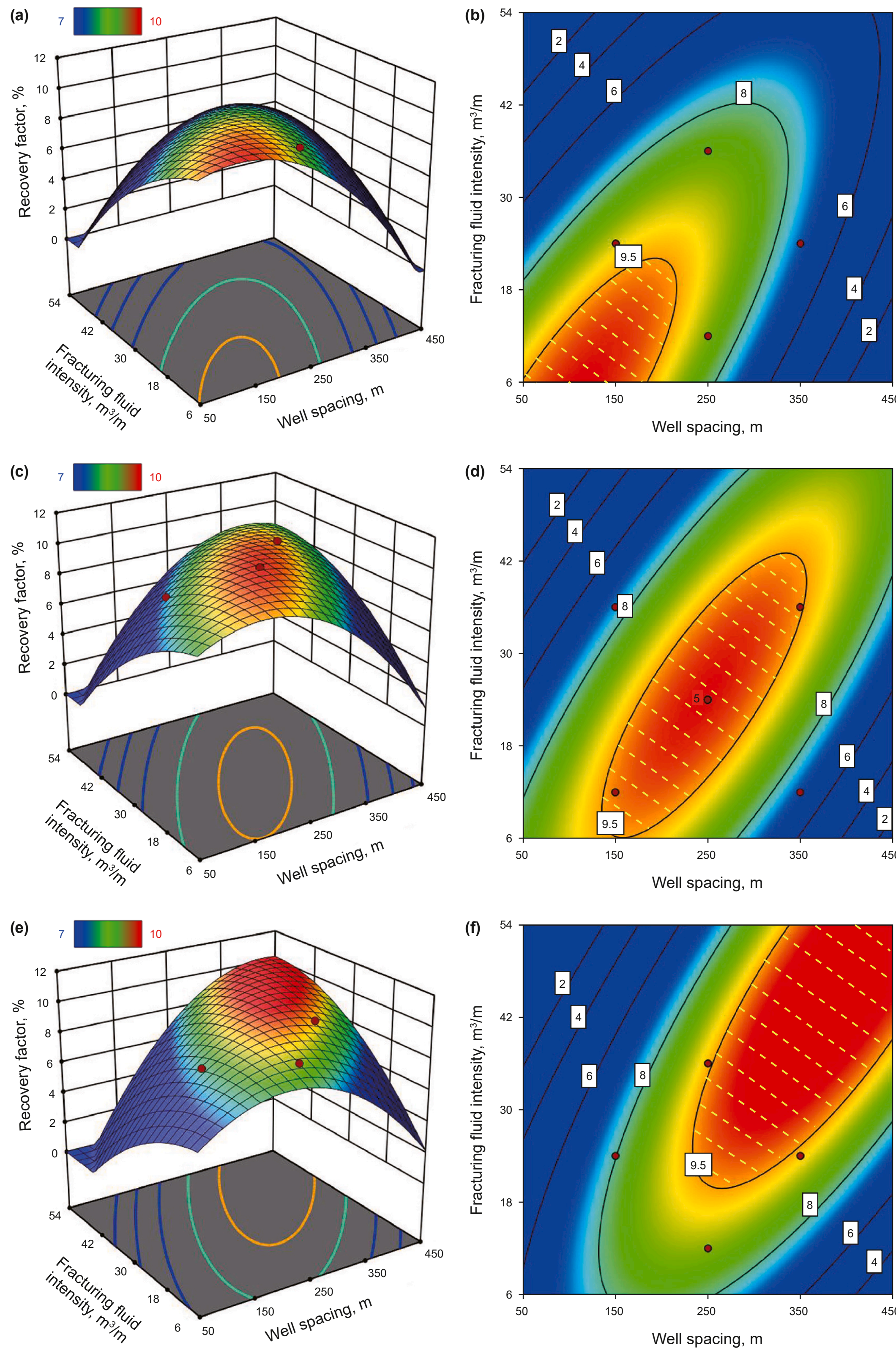

Fig. 16. Response surface and contour plot of the interaction between fracturing fluid intensity and well spacing on recovery factor under different reservoir permeabilities. **(a)**, **(b)** 0.1 mD. **(c)**, **(d)** 0.3 mD. **(e)**, **(f)** 0.5 mD.

well spacing > fracturing fluid intensity, indicating that reservoir conditions are the primary factors determining development effectiveness.

4.4. Three-dimensional response surface and two-dimensional contour plot analysis

The shape of the response surface reflects the interactions between variables. A steep surface indicates that the response variable is sensitive to changes in that factor, while a flat surface suggests a smaller effect. Peaks on the surface indicate parameter combinations that lead to the optimal state of the target variable. Color variations help identify the degree of influence in different regions. Fig. 16 presents the response surface and contour plots showing the interaction between fracturing fluid intensity and horizontal well spacing on recovery factor under different reservoir permeability conditions. The data in the figure are extrapolated from the response surface experiment results.

We consider a recovery factor of 9.5% as the minimum economic recovery factor and have plotted the optimal matching region for well spacing and fracturing intensity under different permeability conditions of the reservoir in the study area. This is represented by the area enclosed by the yellow dashed line and the 9.5% recovery factor contour line on the contour plot. Under the corresponding average reservoir permeability conditions, the well spacing and the matching fracturing intensity in the region can achieve optimal reservoir utilization. For example, when the average reservoir permeability is 0.1 mD, a well spacing of 150 m and a fracturing fluid intensity of 12 m^3/m result in a relatively high recovery factor. Under the current block permeability condition of 0.3 mD, a well spacing of 250 m and a fracturing fluid intensity of 24 m^3/m achieve the highest recovery factor, which reaches 9.93%. The response surface results reflect the combined effects of reservoir permeability, well spacing, and fracturing intensity on pressure propagation and inter-well pressure interference. Higher permeability leads to faster pressure propagation, which requires larger well spacing and stronger fracturing intensity. In contrast, the pressure propagation is slower in lower-permeability reservoirs, a tighter well spacing with moderate fracturing intensity is generally preferred to mitigate inter-well interference and ensure effective drainage. In the next phase of development for the block, recovery factors can be predicted using the fitted quadratic equation based on reservoir characteristics. The optimal well spacing and fracturing intensity matching can be selected using the response surface and contour plots.

5. Conclusions

In this paper, with the help of machine learning methods, we first analyze the production characteristics of tight oil reservoirs and identify the main factors influencing horizontal well productivity, and then we establish an integrated optimization workflow for well spacing and fracturing intensity in tight oil reservoirs. This workflow is applied to a real field reservoir block to explore the optimal matching relationship between well spacing and fracturing intensity under different reservoir permeability conditions and to provide recovery factor prediction correlations. The specific conclusions are as follows:

(1) The water cut of tight oil reservoirs is initially high but declines rapidly, becoming relatively stable after approximately six months of production. The stable water cut is the primary factor influencing the cumulative oil production of horizontal wells in the first year, followed by porosity, proppant intensity, permeability, and fluid intensity. The retention of fracturing fluid cannot be neglected.

(2) An integrated workflow combining modeling, numerical simulation, and optimization is established. The material balance method is used to equivalently represent the retention of fracturing fluid, which aids in early water cut matching. In the study block, under the current fracturing intensity, the optimal well spacing is 250 m. Under the optimal well spacing, the EUR loss is approximately 13% compared to original 400 m well spacing, while the inter-well pressure interference is minimal and utilization degree a high.

(3) The well spacing, fracturing intensity, and reservoir permeability of horizontal wells impact well productivity and controlled oil volume, thereby influencing the recovery factor. The P-value of the quadratic regression model constructed through response surface experiments is less than 0.0001, and the coefficient of determination (R^2) is 0.9833, indicating high significance. This model can be used to predict the recovery factor under different parameter conditions.

(4) Under the current permeability conditions (0.3 mD) of the reservoir block, the highest recovery factor of 9.93% is achieved with a well spacing of 250 m and a fracturing fluid intensity of 24 m^3/m. In areas with lower permeability, it is recommended to use smaller well spacing and a smaller fracturing intensity, while in areas with higher permeability, larger well spacing and a larger fracturing intensity are recommended. The optimal combination can be identified using the response surface contour plot.

CRediT authorship contribution statement

Wen-Sheng Wu: Writing – review & editing, Writing – original draft, Visualization, Software, Methodology, Investigation, Formal analysis, Data curation, Conceptualization. **Bo-Wei Zhang:** Writing – review & editing, Visualization, Software, Investigation, Formal analysis, Data curation, Conceptualization. **Shi-Kai Tong:** Software, Investigation, Formal analysis, Data curation. **Xiu-Kun Wang:** Validation, Supervision, Project administration, Methodology, Funding acquisition.

Conflicts of interests

The authors declare that the research was conducted in the absence of any commercial or financial relationships that could be construed as a potential conflict of interest.

Acknowledgement

This work is supported by National Natural Science Foundation of China (No. U24B6002-05-02 and No. 52204060).

References

Abualfaraj, N., Gurian, P.L., Olson, M.S., 2014. Characterization of Marcellus shale flowback water. Environ. Eng. Sci. 31 (9), 514–524. https://doi.org/10.1089/ees.2014.0001.

Al-Fatlawi, O., Hossain, M., Essa, A., 2019. Optimization of fracture parameters for hydraulic fractured horizontal well in a heterogeneous tight reservoir: An equivalent homogeneous modelling approach. In: SPE Kuwait Oil and Gas Show and Conference, D023S004R008. https://doi.org/10.2118/198185-MS.

Alkouh, A., Wattenbarger, R.A., 2013. New advances in shale reservoir analysis using flowback data. In: SPE Eastern Regional Meeting. https://doi.org/10.2118/165721-MS.

Cai, Y., Dahi Taleghani, A., 2019. Pursuing improved flowback recovery after hydraulic fracturing. In: SPE Eastern Regional Meeting. https://doi.org/10.2118/196585-MS.

Conti, J., Holtberg, P., Diefenderfer, J., LaRose, A., Turnure, J.T., Westfall, L., 2016. International Energy Outlook 2016 with Projections to 2040. USDOE Energy Information Administration (EIA), Washington, DC (United States). https://doi.org/10.2172/1296780.

Edwards, R.W., Doster, F., Celia, M.A., Bandilla, K.W., 2017. Numerical modeling of gas and water flow in shale gas formations with a focus on the fate of hydraulic fracturing fluid. Environ. Sci. Technol. 51 (23), 13779–13787. https://doi.org/10.1021/acs.est.7b03270.

Fowler, G., Ratcliff, D., McClure, M., 2022. Modeling frac hits: Mechanisms for damage versus uplift. In: International Petroleum Technology Conference. https://doi.org/10.2523/IPTC-22194-MS.

Fu, W., Morris, J.P., Fu, P., Huang, J., Sherman, C.S., Settgast, R.R., Ryerson, F.J., 2021. Developing upscaling approach for swarming hydraulic fractures observed at hydraulic fracturing test site through multiscale simulations. SPE J. 26 (5), 2670–2684. https://doi.org/10.2118/199689-PA.

Garcia, A.V., Rached, R.M., Rodriguez-Hernandez, C.D., Santamarina, J.C., 2025. Hydraulic fracture propagation in pre-structured media: Stress field and fracture network topology. Rock Mech. Rock Eng. 59, 3605–3615. https://doi.org/10.1007/s00603-025-05003-8.

Guan, Q., Chen, C., Pu, X., Wan, Y., Xu, J., Zeng, H., et al., 2024. Production performance analysis of a continental shale oil reservoir in Bohai Bay Basin. Petroleum 10 (2), 294–305. https://doi.org/10.1016/j.petlm.2023.11.002.

Guo, D., Kang, Y., Wang, Z., Zhao, Y., Li, S., 2022. Optimization of fracturing parameters for tight oil production based on genetic algorithm. Petroleum 8 (2), 252–263. https://doi.org/10.1016/j.petlm.2021.11.006.

Gupta, I., Rai, C., Devegowda, D., Sondergeld, C.H., 2021. Fracture hits in unconventional reservoirs: a critical review. SPE J. 26 (1), 412–434. https://doi.org/10.2118/203839-PA.

Helmy, A.G., Salem, S.K., Elnoby, M., 2025. Sensitivity analysis of hydraulic fracturing parameters for optimum horizontal well spacing in tight oil reservoirs. Arabian J. Sci. Eng. 50 (7), 4813–4832. https://doi.org/10.1007/s13369-024-09311-z.

Hu, J., Zhang, C., Rui, Z., Yu, Y., Chen, Z., 2017. Fractured horizontal well productivity prediction in tight oil reservoirs. J. Petrol. Sci. Eng. 151, 159–168. https://doi.org/10.1016/j.petrol.2016.12.037.

Hui, G., Chen, Z., Wang, Y., Zhang, D., Gu, F., 2023. An integrated machine learning-based approach to identifying controlling factors of unconventional shale productivity. Energy 266, 126512. https://doi.org/10.1016/j.energy.2022.126512.

Iqbal, M., Zakir, M.M., Mehmood, S., 2023. Reserves estimation and production forecasting using a quick sector modeling technique in tight oil sands – A case study. In: SPE/PAPG Pakistan Section Annual Technical Conference, SPE-217357-MS. https://doi.org/10.2118/217357-MS.

Lei, Z., Dai, K., Dou, X., Shi, J., Chen, Z., Zhu, Z., Tao, Z., 2020. Optimization well spacing for development of shale oil reservoirs using integration of data analytics, geomechanics modeling, pilots, and economic analysis. In: Unconventional Resources Technology Conference, pp. 2483–2502. https://doi.org/10.15530/urtec-2020-3197.

Liu, S., 2023. Review of the development status and technology of tight oil: Advances and outlook. Energy Fuel. 37 (19), 14645–14665. https://doi.org/10.1021/acs.energyfuels.3c02726.

Luo, S., Su, H., 2022. Study on the production decline characteristics of shale oil: Case study of Jimusar field. Front. Energy Res. 10, 845651. https://doi.org/10.3389/fenrg.2022.845651.

Male, F., 2019. Using a segregated flow model to forecast production of oil, gas, and water in shale oil plays. J. Petrol. Sci. Eng. 180, 48–61. https://doi.org/10.1016/j.petrol.2019.05.010.

Male, F., Aiken, C., Duncan, I.J., 2018. Using data analytics to assess the impact of technology change on production forecasting. In: SPE Annual Technical Conference and Exhibition. https://doi.org/10.2118/191536-MS.

Male, F., Duncan, I.J., 2022. The paradox of increasing initial oil production but faster decline rates in fracking the Bakken Shale: Implications for long term productivity of tight oil plays. J. Petrol. Sci. Eng. 208, 109406. https://doi.org/10.1016/j.petrol.2021.109406.

Nolte, D.D., Pyrak - Nolte, L.J., Hopp, C., 2025. Monitoring fracture hydromechanical evolution in the lab and field using unsupervised metric learning. J. Geophys. Res. Mach. Learn. Comput. 2 (3), e2025JH000657. https://doi.org/10.1029/2025JH000657.

Pankaj, P., 2018. Decoding positives or negatives of fracture-hits: A geomechanical investigation of fracture-hits and its implications for well productivity and integrity. In: Unconventional Resources Technology Conference, pp. 3717–3742. https://doi.org/10.15530/URTEC-2018-2876100.

Raterman, K.T., Farrell, H.E., Mora, O.S., Janssen, A.L., Gomez, G.A., Busetti, S., et al., 2018. Sampling a stimulated rock volume: An eagle ford example. SPE Reservoir Eval. Eng 21 (4), 927–941. https://doi.org/10.2118/191375-PA.

Rostamian, A., de Moraes, M.B., Schiozer, D.J., Coelho, G.P., 2025. A survey on multi-objective, model-based, oil and gas field development optimization: Current status and future directions. Pet. Sci. 22 (1), 508–526. https://doi.org/10.1016/j.petsci.2024.09.018.

Sharma, M.M., Manchanda, R., 2015. The role of induced un-propped (IU) fractures in unconventional oil and gas wells. In: SPE Annual Technical Conference and Exhibition. https://doi.org/10.2118/174946-MS.

Tian, C., Lei, Z., Jiang, Q., Chang, T., Chen, D., Lu, Z., Li, S., 2019. Optimizing well spacing and fracture design using advanced multi-stage fracture modeling and discrete fractured reservoir simulation in tight oil reservoir. In: SPE Europec Featured at EAGE Conference and Exhibition. https://doi.org/10.2118/195455-MS.

Tong, S., Wang, F., Gao, H., Zhu, W., 2024. A machine learning-based method for analyzing factors influencing production capacity and production forecasting in fractured tight oil reservoirs. Int. J. Hydrogen Energy 70, 136–145. https://doi.org/10.1016/j.ijhydene.2024.05.036.

Wang, C., Zhu, H., Tang, X., He, M., Kong, F., Li, D., et al., 2024a. Study on post-fracturing inter-well interference in deep shale gas. In: ARMA US Rock Mechanics/Geomechanics Symposium, ARMA-2024-0182. https://doi.org/10.56952/ARMA-2024-0182.

Wang, M., Leung, J.Y., 2015. Numerical investigation of fluid-loss mechanisms during hydraulic fracturing flow-back operations in tight reservoirs. J. Petrol. Sci. Eng. 133, 85–102. https://doi.org/10.1016/j.petrol.2015.05.013.

Wang, Y., Duan, Y., Song, Y., Du, Y., 2024b. Supercritical CO_2-driven intersections of multi-well fracturing fracture network and induced microseismic events in naturally fractured reservoir. Eng. Comput. 41 (10), 2594–2620. https://doi.org/10.1108/EC-01-2024-0079.

Wang, Y., Li, L., Liu, N., 2024c. Frac-hits and connections of multi-well hydro-fracturing fracture network involving the variable factors: Well spacing, perforation cluster spacing and injection rate. Eng. Comput. 41 (6), 1672–1696. https://doi.org/10.1108/EC-01-2024-0077.

Wang, Y., Duan, Y., Wang, D., Ping, E., 2025a. Numerical analysis for center-and edge-type intersections of hydraulic fracture network under varying crossed natural fractures and fluid injection rate. Comput. Part. Mech. 12, 4849–4864. https://doi.org/10.1007/s40571-025-00970-9.

Wang, Y., Liu, X., Liu, N., Duan, Y., Ju, Y., 2025b. Heterogeneous continuum–discontinuum modeling for dynamic diversion and penetration behaviors of hydraulic fractures contacting multi-layers and granules in tight reservoir rock. Comput. Part. Mech. 12 (5), 4065–4087. https://doi.org/10.1007/s40571-025-01045-5.

Wang, Y., Liu, X., Liu, N., Wang, J., 2025c. Deflection behaviours and fractal morphology of hydraulic fractures meeting beddings and granules with variable geometrical configurations and geomechanical properties. Eng. Comput. 42 (4), 1577–1598. https://doi.org/10.1108/EC-02-2024-0131.

Wang, Y., Liu, N., Liu, X., Duan, Y., Chen, X., 2026. Unstable propagation and connection of multicluster hydraulic fractures induced by multiwell hydro-fracturing from the perspective of shear stress shadow disturbance. J. Energy Eng. 152 (1), 04025107. https://doi.org/10.1061/JLEED9.EYENG-6374.

Wang, X., Wu, W., Wang, X., Song, Z., Sheng, J.J., 2025d. Numerical investigating oil-water flow in shale oil reservoirs accounting for fracture swarms and injected hydraulic fluids. Geoenergy Sci. Eng. 247, 213717. https://doi.org/10.1016/j.geoen.2025.213717.

Wu, W., Kakkar, P., Zhou, J., Russell, R., Sharma, M.M., 2017. An experimental investigation of the conductivity of unpropped fractures in shales. In: SPE Hydraulic Fracturing Technology Conference and Exhibition. https://doi.org/10.2118/184858-MS.

Wu, W., Sharma, M.M., 2017. A model for the conductivity and compliance of unpropped and natural fractures. SPE J. 22 (6), 1893–1914. https://doi.org/10.2118/184852-PA.

Wu, W., Song, G., Zhang, H., Wang, X., Song, Z., 2025. Optimization of well spacing with an integrated workflow: A case study of the Fuyu Tight Oil Reservoir in the Daqing Oil Field, China. Processes 13 (4), 1008. https://doi.org/10.3390/pr13041008.

Xiong, H., Liu, S., Feng, F., Liu, S., Yue, K., 2020. Optimizing fracturing design and well spacing with complex-fracture and reservoir simulations: A Permian Basin case study. SPE Prod. Oper. 35 (4), 703–718. https://doi.org/10.2118/194367-PA.

Xiong, H., Wu, W., Gao, S., 2018. Optimizing well completion design and well spacing with integration of advanced multi-stage fracture modeling & reservoir simulation – A Permian Basin case study. In: SPE Hydraulic Fracturing Technology Conference and Exhibition. https://doi.org/10.2118/189855-MS. SPE-189855-MS.

Yang, B., Zhang, H., Kang, Y., You, L., She, J., Wang, K., Chen, Z., 2019. In situ sequestration of a hydraulic fracturing fluid in Longmaxi shale gas formation in the Sichuan Basin. Energy Fuel. 33 (8), 6983–6994. https://doi.org/10.1021/acs.energyfuels.9b00712.

Zhang, K., Tang, M., Du, X., Ma, B., Qiu, K., Wang, L., et al., 2019. Application of integrated geology and geomechanics to stimulation optimization workflow to maximize well potential in a tight oil reservoir, Ordos Basin, northern central China. In: ARMA US Rock Mechanics/Geomechanics Symposium, ARMA-2019-2187.

Zhang, X., Wang, H., Ma, F., Sun, X., Zhang, Y., Song, Z., 2016. Classification and characteristics of tight oil plays. Pet. Sci. 13 (1), 18–33. https://doi.org/10.1007/s12182-015-0075-0.

Zhang, Y., Ge, H., Shen, Y., McLennan, J., Liu, D., Li, Q., et al., 2021. The retention and flowback of fracturing fluid of branch fractures in tight reservoirs. J. Petrol. Sci. Eng. 198, 108228. https://doi.org/10.1016/j.petrol.2020.108228.